Current Biology 20, 1244–1253, July 27, 2010 ©2010 Elsevier Ltd All rights reserved DOI 10.1016/j.cub.2010.06.034

Article

Intercellular Coupling Regulates the Period of the Segmentation Clock

Leah Herrgen,[1] Saúl Ares,[2] Luis G. Morelli,[1,2,3] Christian Schröter,[1] Frank Jülicher,[2] and Andrew C. Oates[1,*]
[1]Max Planck Institute for Molecular Cell Biology and Genetics, Pfotenhauerstraße 108, 01307 Dresden, Germany
[2]Max Planck Institute for the Physics of Complex Systems, Nöthnitzer Straße 38, 01187 Dresden, Germany
[3]Departamento de Fisica, FCEyN, UBA, Pabellón I, Ciudad Universitaria, 1428 Buenos Aires, Argentina

Summary

Background: Coupled biological oscillators can tick with the same period. How this collective period is established is a key question in understanding biological clocks. We explore this question in the segmentation clock, a population of coupled cellular oscillators in the vertebrate embryo that sets the rhythm of somitogenesis, the morphological segmentation of the body axis. The oscillating cells of the zebrafish segmentation clock are thought to possess noisy autonomous periods, which are synchronized by intercellular coupling through the Delta-Notch pathway. Here we ask whether Delta-Notch coupling additionally influences the collective period of the segmentation clock.

Results: Using multiple-embryo time-lapse microscopy, we show that disruption of Delta-Notch intercellular coupling increases the period of zebrafish somitogenesis. Embryonic segment length and the spatial wavelength of oscillating gene expression also increase correspondingly, indicating an increase in the segmentation clock's period. Using a theory based on phase oscillators in which the collective period self-organizes because of time delays in coupling, we estimate the cell-autonomous period, the coupling strength, and the coupling delay from our data. Further supporting the role of coupling delays in the clock, we predict and experimentally confirm an instability resulting from decreased coupling delay time.

Conclusions: Synchronization of cells by Delta-Notch coupling regulates the collective period of the segmentation clock. Our identification of the first segmentation clock period mutants is a critical step toward a molecular understanding of temporal control in this system. We propose that collective control of period via delayed coupling may be a general feature of biological clocks.

Introduction

Many biological clocks are composed of coupled autonomous oscillators [1]. Generally, a population of oscillators with differing autonomous periods can synchronize through coupling, choosing a collective period that is the average of the autonomous periods of individual oscillators [2] (Figure 1A). Examples are coupled chemical systems [3], chirping crickets [4], and flashing fireflies [5]. However, if a significant delay occurs in the coupling, the dynamic effects of the delays may result in novel and complex synchronization phenomena [6, 7]. In particular, the collective period can differ significantly from the average period of autonomous oscillations (Figure 1A). Although this has been studied in mathematical models, and in engineered systems of coupled lasers [8], examples of this scenario have not been identified in biological systems.

The zebrafish segmentation clock may provide an example of such a system. This clock is a population of coupled cellular genetic oscillators in the embryo that drives the sequential subdivision of the presomitic mesoderm (PSM) into multicellular blocks termed somites, with a period of approximately 25 min [9–14]. Upon dissociation, individual PSM cells behave as noisy autonomous oscillators with a range of different periods [11], but within the PSM, neighboring cellular oscillators are synchronized by coupling through the Delta-Notch signal transduction pathway [10, 13, 15, 16] (Figure 2A). Reduction of Delta-Notch coupling results in the gradual decay of segmentation clock synchrony, eventually causing somite boundary defects at a position along the embryonic axis that depends on the remaining strength of the coupling [10, 13, 15]. Given that delays in the coupling on the order of the period are expected from synthesis, trafficking, and transduction of Delta coupling signals [17, 18], it is possible that Delta-Notch coupling causes a collective period in the zebrafish segmentation clock that differs from the average of the autonomous oscillators, in agreement with numerical simulation of gene network models of the zebrafish segmentation clock for several cells [9, 19].

Together with these temporal properties, the segmentation clock also has a spatial aspect. Oscillating gene expression waves propagate through the PSM, forming striped patterns [12]. These patterns of gene expression are consistent with a gradual slowing of autonomous oscillator frequency as cells approach an arrest front in the anterior PSM, a situation that can be described by oscillators with a position-dependent frequency along the PSM [12, 17, 20–25]. We recently introduced a general framework building on previous efforts [13, 17, 21, 22] that combines the spatial and temporal aspects of the segmentation clock and adds delayed coupling between neighboring oscillators [20] (Figure 1B). This delayed coupling theory describes the collective spatiotemporal behavior of the tissue arising from properties of individual cells, which are modeled as phase oscillators. Because the delayed coupling theory has a relatively small number of parameters, most of which can be measured from the developing embryo, it is well suited to fit experimental data. The oscillating gene expression patterns described by the theory are in good quantitative agreement with experimental data from wild-type embryos [17, 20]. Importantly, this approach permits the quantitative experimental analysis of changes to the pattern's wavelength induced by altered collective period or frequency profile [20].

According to this theoretical work, if significant time delays exist in Delta-Notch coupling, then reduction of this coupling will change the collective period of the segmentation clock. This is expected to give rise to three defining phenotypes in the embryo: (1) an altered somitogenesis period [9, 19, 20],

*Correspondence: oates@mpi-cbg.de

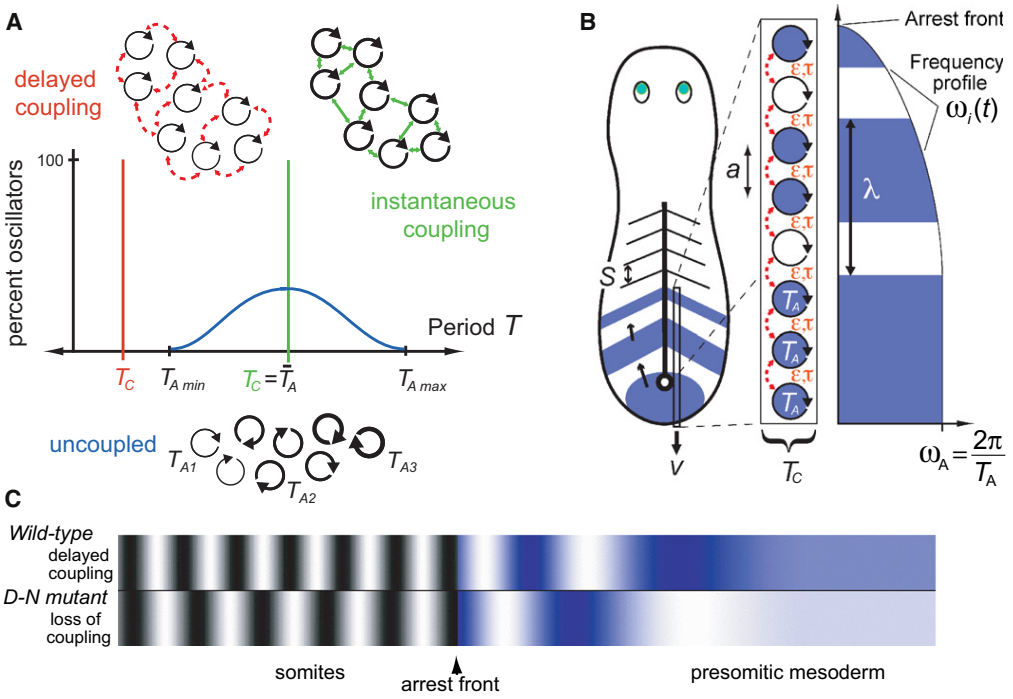

Figure 1. Theoretical Description of Collective and Spatial Properties of Oscillators in the Segmentation Clock

(A) Delayed coupling can alter collective period. Uncoupled oscillators with random phase and unimodal symmetric distribution of autonomous periods T_{A1}, T_{A2}, … (blue line) with average period $\overline{T}_A$. Synchronization by instantaneous weak coupling (green arrows) results in a collective period $T_C = \overline{T}_A$. Synchronization by delayed coupling (red arrows) can result in T_C different to $\overline{T}_A$. Shortening or lengthening of T_C relative to $\overline{T}_A$ is possible depending on the value of the delay.

(B) The delayed coupling theory describes the segmentation clock as an array of coupled phase oscillators [20]. The key features are (1) a posterior front describing embryonic elongation with velocity v, comoving with a front that arrests oscillations on the anterior side of the PSM; (2) local coupling of oscillators, with strength ε, accounting for Delta-Notch intercellular coupling; (3) a time delay τ in coupling, due to synthesis and trafficking of molecules; (4) a frequency profile $\omega_i(t)$ across the PSM accounting for the slowing of cellular oscillators as they approach the arrest front, characterized by decay length ρ and the period of the fastest autonomous oscillators T_A, located in the posterior PSM.

(C) Snapshot from Movie S1 generated with the analytical solution to the delayed coupling theory continuum approximation with experimentally determined parameters from this work, predicting that loss of coupling results in increased segment length and wavelength of the oscillatory pattern.

(2) a correspondingly altered segment length due to the change in period [12, 17, 20–22, 26–28], and (3) corresponding changes to the expression pattern wavelength of oscillating genes in the PSM [20] (Figure 1C; Movie S1, available online). In addition, the delayed coupling theory predicts that there are values of the coupling delay for which a dynamic instability occurs [20], destabilizing the spatial patterns of gene expression. In this work we experimentally confirm these predictions and use the delayed coupling theory to estimate from our data the period of the autonomous oscillations, the coupling strength, and the time delay in the coupling. Together, these findings show that the segmentation clock's collective period is regulated by the Delta-Notch pathway and support a role for delayed coupling in setting the collective period of biological clocks.

Results

Somitogenesis Period Is Increased by Reduction of Delta-Notch Coupling

An altered segmentation clock period is expected to alter the period of somitogenesis. To test whether reduced Delta-Notch coupling alters the period of somitogenesis, we analyzed conditions affecting this signaling pathway. These were mutants for the Delta ligands *after eight* (*aei/deltaD*) and *beamter* (*bea/deltaC*), the Notch receptor *deadly seven* (*des/notch1a*), and the E3 ubiquitin ligase *mind bomb* (*mib*) involved in Delta trafficking, as well as embryos treated with DAPT, a γ-secretase inhibitor that attenuates Notch receptor function [10, 13] (Figure 2A, Experimental Procedures). Somitogenesis period was measured in live embryos via our high-precision time-lapse microscopy protocol [14, 29]. Somitogenesis period was increased to 119% ± 2% (mean ± 95% confidence interval [CI]) in *mib* (Figures 2B–2E; Movies S2 and S3), to 123% ± 4% in *aei/deltaD*, and to 107% ± 3% in *des/notch1a* embryos (Figure 2E) as compared to their wild-type siblings. The increase was constant until, as the result of a loss of synchrony, intact somite boundaries no longer formed (Figure 2C) [13, 15]. Blocking Notch signaling with saturating DAPT concentrations (≥40 μM) [13] increased somitogenesis period to 118% ± 1% of control (Figure 2E), indicating that the smaller change in *des/notch1a* is probably due to Notch receptor redundancy [13].

The morphology of the forming anterior somite boundaries in *bea/deltaC* embryos is less regular than with DAPT treatment and in the other Delta-Notch mutants [30, 31], and this prevented precise measurement of somitogenesis period in our assay. Although *bea/deltaC* and DAPT treatment yield the same desynchronization phenotype, indicating an equivalent quantitative contribution to coupling within the clock [13, 32, 33], the combined observations on anterior

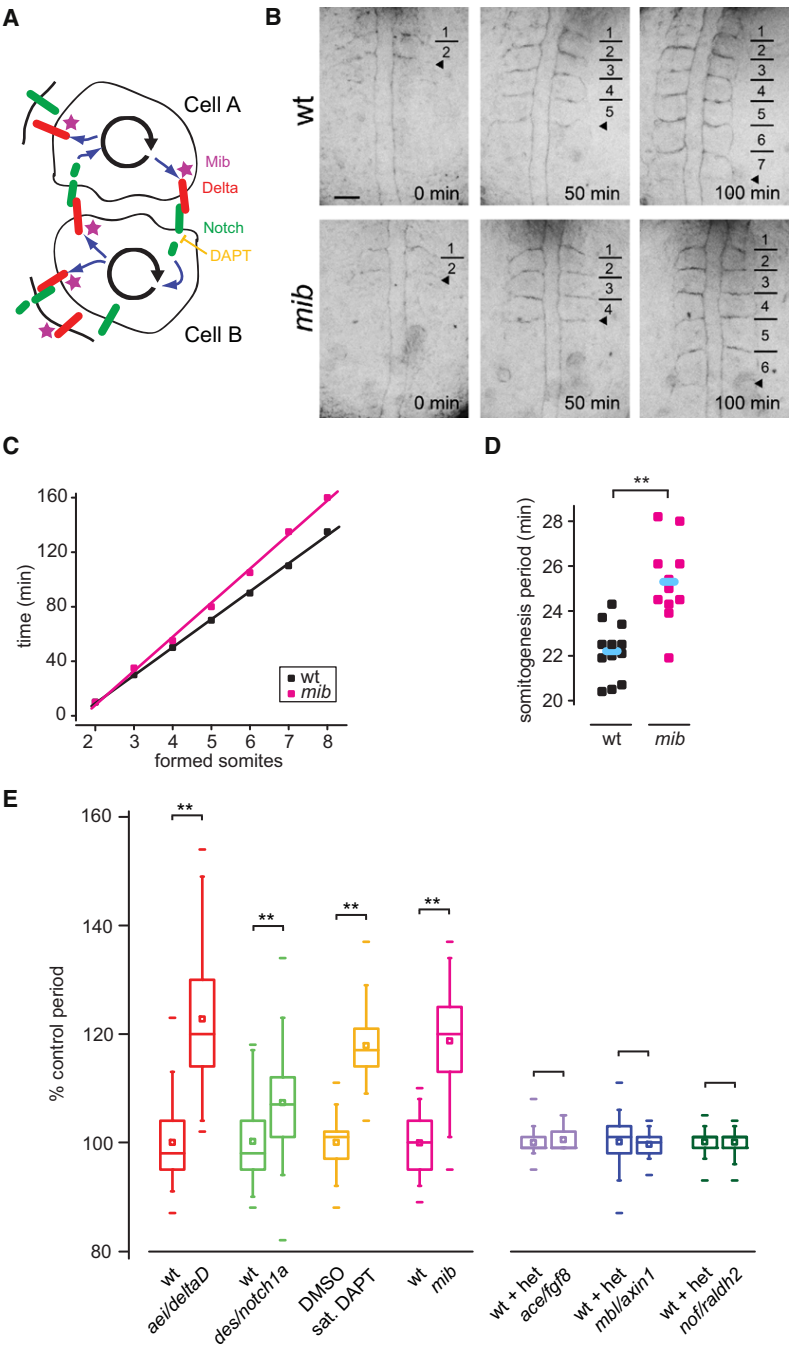

Figure 2. Somitogenesis Period Increases after Reduction in Delta-Notch Coupling

(A) Delta-Notch coupling between two oscillating PSM cells. Delta is the ligand for the Notch receptor, which can be inhibited via the small molecule DAPT. Mib is a ubiquitin ligase required for Delta trafficking and activation.

(B) Time-lapse movies of wild-type (wt) and *mib* embryos. Bars indicate formed somite boundaries; arrowheads indicate forming boundaries. Dorsal view is anterior to top. The scale bar represents 50 μm.

(C) Time versus somite number plot for (B). Linear fits of data (R^2 [wt and *mib*] = 0.999) yield somitogenesis periods of 20.5 min (wt) and 25.0 min (*mib*).

(D) Distribution of somitogenesis periods in the experiment from which (B) and (C) were taken (n [wt] = 12, n [*mib*] = 11). Blue bars indicate mean somitogenesis period. Temperature = 28.2 ± 0.1°C.

(E) Box-and-whisker plots of somitogenesis period: n ≥ 37 total embryos, more than six independent trials per experimental condition, except *ace/fgf8*, *mbl/axin1*, and *nof/raldh2*, for which n ≥ 16 total embryos, two independent trials per experimental condition. het denotes heterozygote. **p < 0.001, Student's t test. Figures S1 and S2 show that general developmental rate is unaffected in the conditions with slower period. The central box covers the interquartile range with the mean indicated by the small square and the median by the line within the box. The whiskers extend to the 5th and 95th percentiles, and small bars depict the most extreme values.

somite boundary morphology suggest an additional, γ-secretase inhibitor-insensitive role for *bea/deltaC* in somite boundary formation downstream of the segmentation clock.

We detected no change in general developmental rate and tissue differentiation (Figure S1) or in embryonic axial elongation rate (Figure S2) in the Delta-Notch mutant or DAPT-treated embryos, consistent with previous studies [31, 34]. This argues against general slowing of development as an explanation for increased somitogenesis period. Fibroblast growth factor (FGF), Wnt, and retinoic acid (RA) signaling are required for aspects of vertebrate somitogenesis but are not implicated in coupling, as reviewed in [35]. We measured somitogenesis period in *acerebellar* (*ace/fgf8*), *masterblind* (*mbl/axin1*), and *no fin* (*nof/raldh2*) mutants, which affect the FGF, Wnt, and RA pathways, respectively, and detected no change (Figure 2E). Although not excluding roles for these pathways in period setting, these results indicate that increased somitogenesis period is not a general consequence of defective intercellular PSM signaling pathways. We conclude that Delta-Notch coupling regulates somitogenesis period.

Segment Length Is Increased by Reduction of Delta-Notch Coupling

Segment length in the elongating embryo is thought to be determined by interaction of the segmentation clock and a posteriorly moving wavefront of rapid cell change that arrests oscillations at the anterior end of the PSM [26, 27, 35]. In this Clock and Wavefront model, if the segmentation clock's rhythm is translated directly into spatial periodicity, then the resulting segment length is given by $S = vT_C$, with segment length S, arrest front velocity v, and the segmentation clock's collective period T_C [12, 17, 20–22, 26–28]. Embryonic axial elongation rate and the posterior border of the *mespb* gene expression domain, which we use to define the arrest front location within the PSM [36], were not significantly different between control and Delta-Notch impaired embryos throughout the time of interest (Figure S3, Movies S4 and S5), showing that arrest front velocity was unchanged. Consequently, with an increased segmentation clock period, we expect longer segments. Anterior-posterior length of somites 2–5 was increased in live *mib*, *aei/deltaD*, and DAPT-treated embryos

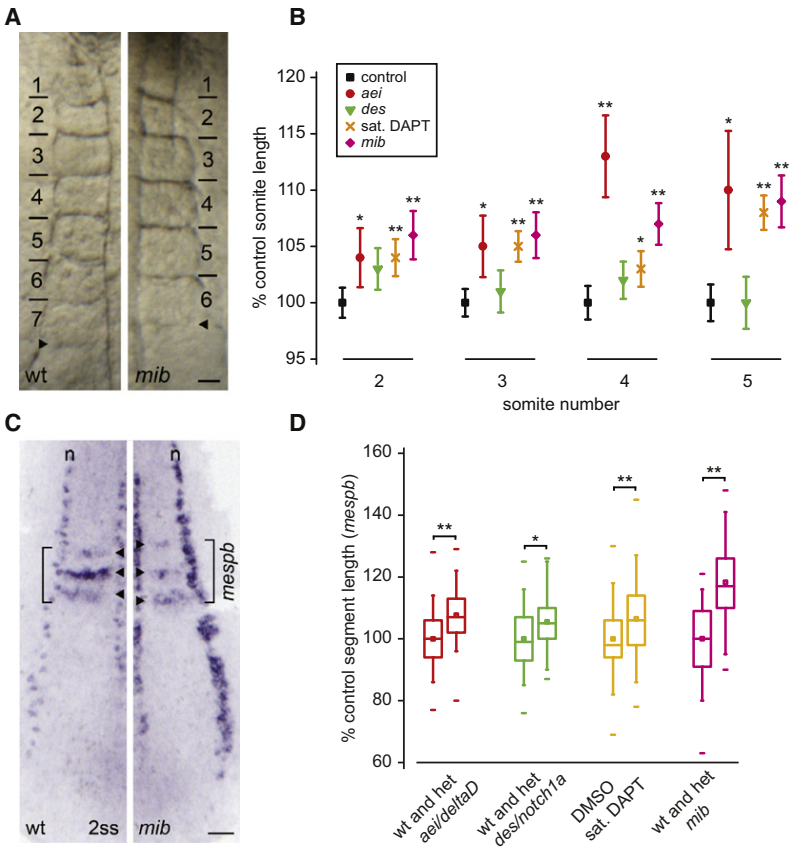

Figure 3. Segment Length Increases after Reduction in Delta-Notch Coupling

(A) Somites of six-somite-stage live embryos. Bars indicate formed somite boundaries; arrowheads indicate forming boundaries. Dorsal view is anterior to top. The scale bar represents 25 μm.

(B) Somite lengths (mean ± 95% CI), n ≥ 40 total embryos per experimental condition, except n = 14 for somite five in *aei/deltaD*, six independent trials per experimental condition. For control population, the largest CI detected is displayed.

(C) In situ hybridization of *mespb* (arrowheads) and *isl1* (interneurons, Rohon-Beard neurons, n). The scale bar represents 50 μm.

(D) Box-and-whisker plots of segment length, n ≥ 40 total embryos, more than three independent trials per experimental condition. *p < 0.01, **p < 0.001, Student's t test. Figure S3 shows that the position of the arrest front in the PSM is unchanged in the conditions with increased segment length. The central box covers the interquartile range with the mean indicated by the small square and the median by the line within the box. The whiskers extend to the 5th and 95th percentiles, and small bars depict the most extreme values.

versus wild-type siblings (Figures 3A and 3B), but in *des/notch1a* embryos, which had the smallest period change, we detected no alteration of somite length (Figure 3B). Assaying the distance between *mespb* expression stripes, which we use to mark segment length at the arrest front before somite formation [36], revealed an increase in segment length in *mib*, *aei/deltaD*, *des/notch1a*, and DAPT-treated embryos (Figures 3C and 3D). We conclude that Delta-Notch coupling has an effect on segment length.

Spatial Patterns of Oscillating Cells Are Altered in *mind bomb* Mutants

If the changes we observed in somitogenesis period are produced by an altered collective period T_C of the segmentation clock, then we should find corresponding changes to the gene expression patterns in the PSM. These changes can be quantified [20] and should provide an independent, gene-expression-based estimate for the period change measured in our time-lapse experiments. To test this prediction, we quantified stripe wavelength in *mib* mutant embryos, finding a systematic increase in wavelength for a given position as compared to wild-type siblings (Figures 4A and 4B). Fitting the delayed coupling theory to the data (Figure 4B; Experimental Procedures) indicated an increase in normalized segment length s of 116% ± 1% in *mib* embryos while leaving the frequency profile unchanged (Figure 4C). Because arrest front velocity is not altered in the mutant, $S = vT_C$ indicates a change to collective period similar to that obtained from somitogenesis period measurement (119% ± 2%, Figure 2).

In summary, we have shown that conditions reducing Delta-Notch signaling lead to corresponding changes in (1) somitogenesis period and (2) segment length, without changes to arrest front velocity. In addition, (3) we find changes to oscillating gene expression patterns in the PSM consistent with changes in collective period (Table 1). Combined, our findings indicate a change in the segmentation clock's collective period as a result of reduced Delta-Notch coupling. This is as expected if significant delays exist in the coupling. The magnitude of these changes, ~10%–20% of the wild-type period, is similar to those resulting from single gene mutations in the circadian clock [37–40].

Estimation of Autonomous Period, Coupling Strength, and Coupling Delay from the Data

In order to understand these collective period changes in terms of the strength and delay in coupling between PSM cells, we again use the delayed coupling theory [20]. The collective period T_C is related to the period T_A of uncoupled autonomous oscillators in the posterior PSM, a positive coupling strength ε, and a coupling delay τ by

$$\frac{2\pi}{T_C} = \frac{2\pi}{T_A} - \varepsilon \sin\left(\frac{2\pi}{T_C}\tau\right). \quad (1)$$

Note that the coupling strength ε and coupling delay τ are effective parameters of a tissue-level theory. Therefore, their values are not necessarily related in simple ways to molecular quantities such as the number of molecules involved in coupling or duration of a molecular signaling event. Nevertheless, their values depend on underlying molecular processes, and changes to these processes cause corresponding changes to the effective parameters (Experimental Procedures). The effects of delayed coupling on collective period in Equation 1 are illustrated with the following gedankenexperiment: if two uncoupled oscillators cycling at the same pace with equal phases are suddenly coupled with a delay, they will receive information about the phase of the other oscillator from an earlier time point. The oscillators will change period as

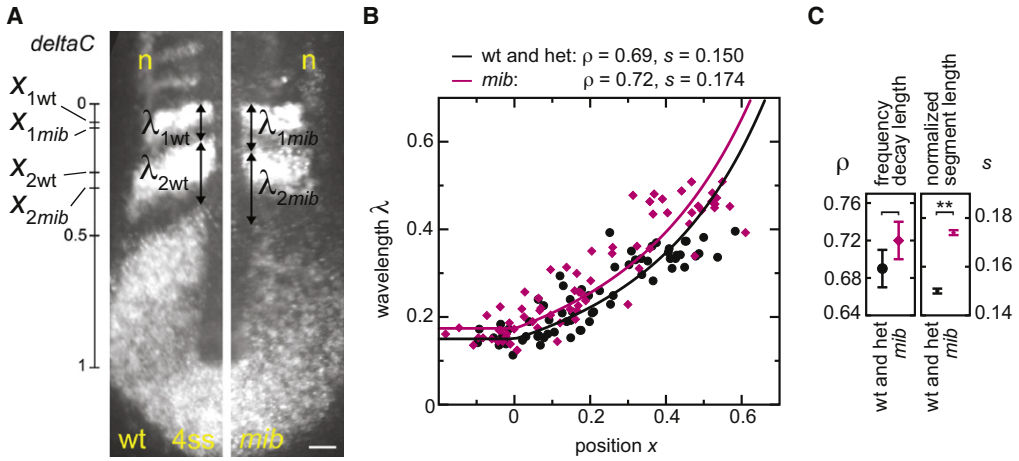

Figure 4. Determination of Segmentation Clock Collective Period from Oscillating Gene Expression Patterns

(A) In situ hybridization: *deltaC* and *isl1* (interneurons and Rohon-Beard neurons, n) in representative wild-type and *mib* embryos. The scale bar represents 50 μm.

(B) Measurements of normalized gene expression wavelength λ and position x; wild-type is black and *mib* is pink. Data points: n (wt) = 65, 28 embryos, n (*mib*) = 70, 28 embryos, two independent trials. Curves indicate fit of Equation 3 to data (Experimental Procedures).

(C) Values of frequency profile decay length ρ, and normalized segment length s parameters from the fit to the data. Error bars show 95% CI from bootstrap analysis (Supplemental Experimental Procedures 2.2.5). **p < 0.001, Student's t test.

they try to synchronize to the apparent (delayed) phase of their neighbor. Depending on the relative value of the delay and the autonomous period, this could result in slowing or speeding of the oscillators. As this process occurs across a population, a collective period self-organizes.

Equation 1 predicts a continuous variation of collective period, and therefore somitogenesis period, with coupling strength. We tested this prediction by determining the response of somitogenesis period to varying DAPT concentrations and found a variation up to saturation consistent with a smooth change of the collective period (Figure 5A).

For a given autonomous period T_A, the collective period T_C described by Equation 1 depends on coupling strength ε and coupling delay τ in a complex way (Figure 5B), analogous to that described in models of gene regulatory networks with delay in the coupling [41]. As the time delay is varied, branches of stable synchronized oscillations are separated by unstable branches where synchrony is lost (Figure 5B). To locate the situation corresponding to the wild-type zebrafish segmentation clock in this diagram, we estimated parameters ε and τ by fitting the delayed coupling theory to our experimental data (Figure 5A, Experimental Procedures). For this purpose, we assume that saturating DAPT completely blocks coupling [13] and that a loss of coupling does not affect T_A over relevant time scales [13, 15]. From our time-lapse experiments, the measured value of $T_A \approx 1.18T_C$ (Figure 2E), which for the zebrafish embryo at 28°C [14] yields $T_A = 28 \pm 1$ min. This value is consistent with independent estimates for T_A from genetic network models [9, 19]. To account for the measured change in period, coupling strength must be at least 0.043 min^{-1} (Equation 1), and from the fit, we estimate coupling strength $\varepsilon = 0.07 \pm 0.04$ min^{-1}. Multiple values of the coupling delay τ are consistent with the wild-type collective period $T_C = 23.5$ min (Figure 5B, dotted line). We use the only value of τ for which the wave pattern is both stable and unique for the determined values of T_A and ε, which is found on branch 2 (Figure 5B), and so estimate coupling delay $\tau = 21 \pm 2$ min, corresponding to $0.9T_C$.

The various experimental perturbations of the Delta-Notch pathway can be consistently mapped to distinct points in a diagram relating collective period and coupling delay (Figure 5C). This map uses the assumption in accordance with previous work [9] that most of the delay in Delta-Notch signaling in the segmentation clock arises from the synthesis and trafficking of Delta molecules in the signal-sending cell [18] and that signal transduction via the cleavage of the Notch intracellular domain is on a shorter time scale [42]. Thus, all mutants and treatments studied here affect the coupling strength, which can be estimated from the onset of segmental defects caused by the gradual desynchronization of the segmentation clock's cells [10, 13, 15, 16], but only *aei/deltaD* and *mib* affect the coupling delay in addition. The *mib* mutant, with reduced endocytic trafficking of Delta in the signal-sending cell [43], shows a strong collective period change despite exhibiting the weakest somite boundary disruption phenotype of any mutant (Table 1), suggesting that coupling delay is strongly increased but coupling strength is only mildly affected. Heterozygote *mib* embryos show an increased period without any somite defects (Figure S4), suggesting that the coupling delay depends sensitively on the level of Mib protein.

Mind Bomb Overexpression Drives the System into Instability

A key prediction of the delayed coupling theory is the existence of instabilities for certain values of the coupling delay. In particular, the instability that separates branch 1 from branch 2 should be reached by reducing the coupling delay from the wild-type value of 21 min to about 16 min (Figures 5B and 5C). Given that reduced levels of Mib increase coupling delay, we reasoned that elevated levels of Mib might offer a way to shorten the delays and thereby experimentally test the existence of the predicted instability. We first performed numerical simulations of the PSM by using the delayed coupling theory with wild-type parameters determined in this work. We found an excellent agreement with the spatial

Table 1. Segmentation Variables in Delta-Notch Mutant and DAPT-Treated Embryos

Experimental Condition	% Control Period[b] (time-lapse analysis)	% Control Somite Length[c] (5th somite)	% Control Segment Length[d] (*mespb* pattern)	% Control Period[e] (*deltaC* stripe wavelength)	Anterior Limit of Segmental Defects
aei/deltaD	123 ± 4[a]	110 ± 5	108 ± 2	n.d.[f]	7 ± 2 [31]
des/notch1a	107 ± 3	100 ± 2	105 ± 3	n.d.	7 ± 2 [13, 31]
sat. DAPT	118 ± 1	108 ± 2	106 ± 2	n.d.	5.2 ± 0.2 [13]
mib	119 ± 2	109 ± 2	118 ± 5	116 ± 1	10–12 [57]

[a] Mean ± 95% CI.
[b] Period measurements: *aei/deltaD*, n (wt) = 46, n (mutant) = 50, six independent trials; *des/notch1a*, n (wt) = 37, n (mutant) = 49, six independent trials; saturating DAPT, n (DMSO) = 114, n (sat. DAPT) = 141, 12 independent trials; and *mib*, n (wt) = 64, n (mutant) 73, eight independent trials.
[c] Somite length measurements (5th somite): *aei/deltaD*, n (wt and het) = 78, n (mutant) = 14; *des/notch1a*, n (wt and het) = 112, n (mutant) = 43; sat. DAPT, n (DMSO) = 104, n (sat. DAPT) = 74; and *mib*, n (wt and het) = 91, n (mutant) = 47, 6 independent trials.
[d] Segment length measurements: *aei/deltaD*, n (wt and het) = 132, n (mutant) = 69, 4 independent trials; *des/notch1a*, n (wt and het) = 80, n (mutant) = 41, 3 independent trials; sat. DAPT, n (DMSO) = 155, n (sat. DAPT) = 239, 8 independent trials; and *mib*, n (wt and het) = 40, n (mutant) = 40, 4 independent trials.
[e] Stripe wavelength measurements: *mib*, n (wt and het) = 65 data points from 28 embryos, n (mutant) = 70 data points from 28 embryos, 2 independent trials. The largest CIs in control populations were 100% ± 2% for period and somite length, 100% ± 4% for segment length, and 100% ± 4% for stripe wavelength in *mib*.
[f] n.d. denotes not done.

organization of *dlc* expression in the wild-type embryo that can be quantified by comparing autocorrelation functions (Figures 6A–6C; Experimental Procedures). We next repeated the simulation with reduced coupling delay. We found that as the system approaches the instability, the normal striped gene expression patterns develop a characteristic disrupted pattern with a range of spatial wavelengths resulting in a flattened average autocorrelation function (Figures 6D and 6E; Figure S5). To test this prediction in vivo, we injected *mib* mRNA into the embryo and assayed the resulting spatial features of cyclic *dlc* expression in the PSM. We found that elevated Mib levels resulted in a disruption of somitogenesis in otherwise normally developing embryos accompanied by a disrupted pattern of *dlc* expression with an autocorrelation function in quantitative agreement with simulations of reduced delay (Figures 6D and 6E; Figure S6). These patterns are distinct from those observed in the loss-of-coupling mutants *aei/deltaD*, *des/notch1a*, and *mib* (Figure S7). These data provide evidence of the predicted delay-dependent dynamic instability and give further support to the existence of delays in Delta-Notch coupling in the zebrafish segmentation clock.

Discussion

Our work in this paper was motivated by theoretical results suggesting that systems of oscillators with time delays in the coupling could tick with a collective period different from the period of the autonomous oscillators (Figure 1). Coupling by Delta-Notch signaling in the zebrafish segmentation clock was an attractive candidate system to observe such effects because the clock's period is of the same order as the expected signaling delays. Here we describe that a reduction in Delta-Notch coupling increases somitogenesis period (Figure 2), produces longer segments (Figure 3), and lengthens the wavelength of oscillating gene expression stripes (Figure 4) in an otherwise normally developing embryo. For this study, the use of multiple-embryo time-lapse imaging [14, 29] was critical to sensitively and precisely measure the timing of

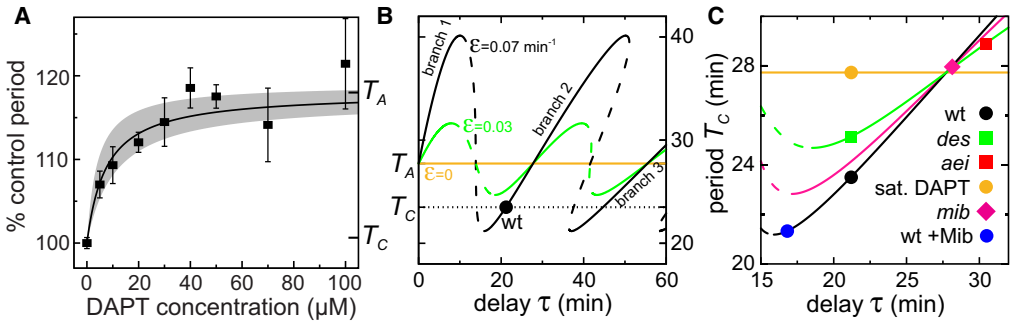

Figure 5. Coupling Strength and Time Delays Regulate the Collective Period of the Segmentation Clock

(A) Somitogenesis period (mean ± 95% CI) versus DAPT concentration: n ≥ 38, more than four independent trials for data points except 70 and 100 μM, for which n ≥ 18, two independent trials. The curve is fit to the delayed coupling theory yielding $\varepsilon = 0.07 \pm 0.04$ and $\tau = 21 \pm 2$ min (Equation 4, Experimental Procedures). The shaded area indicates the error of the fit.

(B) Diagram of solutions to Equation 1. The lines indicate the collective period T_C versus coupling delay τ for different values of coupling strength ε, as indicated. Stable and unstable solutions are indicated by solid and dashed lines, respectively. The dotted line indicates wild-type T_C, 28°C.

(C) Close-up of (B): approximate positions of experimental conditions in parameter space (Supplemental Experimental Procedures 2.2.7). The black dot indicates wild-type, ten-somite stage, 28°C; the blue dot refers to experiments with elevated Mib levels in Figure 6. Because the anterior limit of defects (ALD) of *mib* is between those of wild-type and *des/notch1a*, its coupling strength ε is assumed to be between wild-type and *des/notch1a*. The ALD of *aei/deltaD* is similar to *des/notch1a*; hence, their coupling strengths are similar. The lines indicate T_C versus τ relation for black $\varepsilon = 0.07$ min^{-1}, pink $\varepsilon = 0.05$ min^{-1}, green $\varepsilon = 0.03$ min^{-1}, and orange $\varepsilon = 0$ min^{-1}. Figure S4 shows that *mib* heterozygote embryos have a longer period.

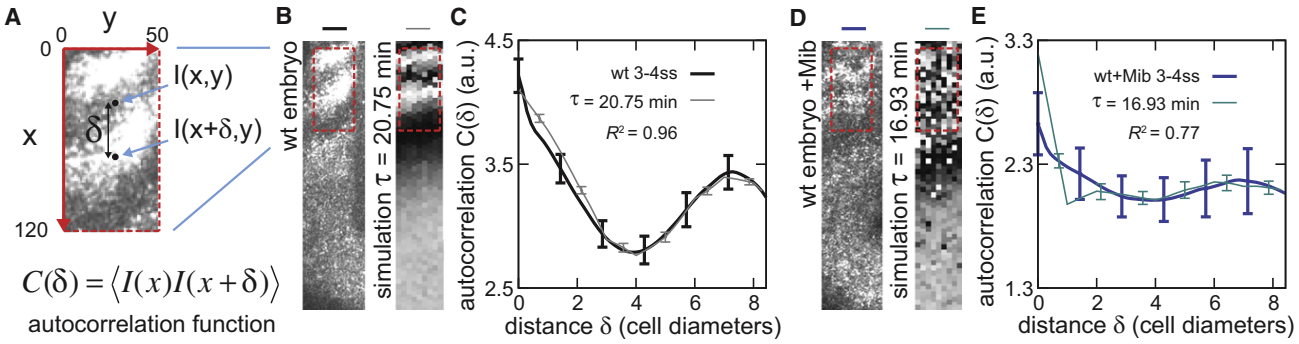

Figure 6. Coupling Time Delays Regulate the Stability of the Segmentation Clock

(A) Schematic of how the autocorrelation function (Equation 6, Experimental Procedures) is computed. A magnification of the gene expression pattern from (B) is shown, together with the reference axes x and y in pixels, and the distance δ between two sample points of gene expression intensity *I*.

(B) Representative cyclic *dlc* expression in PSM of wild-type embryo and DCT simulation with wild-type parameters defined in this work, black dot in Figure 5C.

(C) Average autocorrelation function of spatial patterns in red box from (B): n (embryos) = 15, black line; n (simulations) = 20, gray line. Error bars show standard error of the mean (SEM).

(D) Representative experimental Mib overexpression (400 pg mRNA) and corresponding DCT simulation with reduced coupling delay, blue dot in Figure 5C.

(E) Average autocorrelation function of spatial patterns in red box from (D): n (embryos) = 8, dark blue line; n (simulation) = 20, light blue line. The arbitrary units in the correlation axis are multiplied by 10^{-3}. Figures S5 and S6 show the autocorrelations for decreasing delays in numerical simulations and increasing levels of Mib overexpression in the embryo, and Figure S7 shows that the Delta-Notch loss-of-coupling mutants have autocorrelation functions distinct from Mib overexpression. Error bars show SEM.

somitogenesis and growth in live embryos under controlled conditions. Combined, these experimental results are compelling evidence of a role for Delta-Notch signaling in controlling the period of the segmentation clock.

We analyzed the role of the Delta-Notch intercellular signaling system in regulating the period with the delayed coupling theory [20], which describes the segmentation clock in a simplified way at a cellular and tissue level as a spatially distributed population of phase oscillators with time delays in the coupling. According to theory, collective period is modulated through perturbation of coupling if there are time delays in the coupling [6, 7, 9, 19, 20]. The existence of coupling delays in the segmentation clock is supported by the fit of the delayed coupling theory to the data from the change in collective period with coupling strength (Figure 5), as well as the successful numerical simulation of the oscillating gene expression patterns of the wild-type PSM (Figure 6) using the values of autonomous period, coupling strength, and coupling delay obtained from the fit. Further support for a critical role of coupling delay in the system comes from the experimental observation of a predicted instability consistent with shorter delays (Figure 6). This comparison of spatial patterns of cyclic gene expression in experiment and simulation using an autocorrelation function introduces a novel method for the analysis of perturbation to the segmentation clock. Together, the fit of theory and experimental data in this work gives strong support to the existence and period-setting function of delays in Delta-Notch coupling in the segmentation clock.

Phase oscillators have been shown to correctly capture the dynamics of gene regulatory network models of the segmentation clock [23]. Building such models is one of the important goals of the field [9, 19, 23, 24, 44–46], but the experimental measurement of the many rate parameters of these models is currently difficult in vivo. In contrast, most parameters of the delayed coupling theory, such as collective period, arrest front velocity, segment length, and frequency profile, can be measured from the embryo directly or have been estimated previously [14, 20], leaving autonomous period, coupling strength, and coupling delay to be obtained in this work from the fit of the theory to the new data (Figure 5). The main use of the values we estimate for the effective parameters coupling strength and coupling delay is in the quantitative comparison of experimental situations. Future work may connect these parameter values to measurable events described in detailed molecular models. In contrast, the autonomous period is a simple biological parameter that can be directly tested by methods with cellular resolution of the dynamics.

Our discovery of segmentation period mutants in an intercellular signaling system provides insight into the fundamentally multicellular organization of the segmentation clock. Whereas it was previously recognized that coupling in the zebrafish segmentation clock synchronizes the phases of the oscillating cells of the PSM [10, 13, 15, 16], the results here indicate that the time cost of coupling using macromolecules causes an additional, novel effect—a self-organized regulation of the collective period. This phenomenon is probably not restricted to the segmentation clock; any system where oscillators are coupled with delays of the order of the period should show similar effects. One biological candidate system is the circadian clock, in which cellular rhythms are synchronized by VIP signaling, and where loss of this coupling alters the period [47, 48]. A similar situation may occur in other multicellular systems with coordinated oscillations such as the neuroepithelium and hair follicles [49, 50]. The role of collective effects in controlling the period of other biological clocks now awaits investigation.

Experimental Procedures

In this section we provide a brief outline of the methods that we introduce and use in this work. This material, plus a more comprehensive description and extensive technical details, is provided in corresponding sections in the Supplemental Information. Embryology, microscopy, and molecular biology are covered in section 2.1 and theoretical methods and parameter fitting are covered in section 2.2.

Embryology, Microscopy, and Molecular Biology

Zebrafish embryos were obtained via standard procedures [51]. Mutant alleles were *aei*^{tr233} [52], *bea*^{tm98} [30], *des*^{p37a} [53], *mib*^{ta52b} [43], *ace*^{ti282a} [54], *mbl*^{tm013} [55], and *nof*^{u11} [56], and DAPT treatment was according to [13]. Time-lapse recordings and estimation of somitogenesis period were according to [14, 29], and in situ hybridization was according to [33]. Statistical significance in somitogenesis period, somite and segment length, axial elongation rate, and position of the arrest front was assessed with Student's t test, two-sided, unequal variance. In vitro synthesis of *mib* and *GFP* mRNA was carried out as previously described [32], quantified with a Nanodrop1000 spectrophotometer (Thermo Scientific), and delivered in varying amounts to one-cell-stage embryos via our quantitative injection protocol [13]. After injection, embryos were left to develop until they reached the 3–4 somite stage, when they were fixed for in situ hybridization.

Theoretical Methods and Parameter Fitting

Overview of the Delayed Coupling Theory

The delayed coupling theory (DCT) describes the PSM as an array of coupled phase oscillators and has been previously introduced in detail [20]. The state of oscillator i at time t is described by a phase variable $\theta_i(t)$ whose dynamics is given by

$$\frac{d\theta_i(t)}{dt} = \omega_i(t) + \frac{\varepsilon_i(t)}{N_i}\sum_k \sin[\theta_k(t-\tau) - \theta_i(t)] + \eta\zeta_i(t). \quad (2)$$

The frequency profile $\omega_i(t)$ describes the slowing down of oscillators as they get closer to the arrest front, where oscillations stop. Oscillators are coupled to their neighbors with a coupling strength $\varepsilon_i(t)$, and a delay τ accounts for the finite time introduced by synthesis and trafficking of ligands in the cells sending the signal. Oscillator i is coupled to its N_i nearest neighbors, labeled by k. The zero average uncorrelated random term ζ_i represents different noise sources with total noise strength η.

Parameter Estimation from Cyclic Stripe Wavelength Fitting

Cyclic gene expression patterns are related to the frequency profile in the DCT. To fit these patterns, it is convenient to use the continuum approximation to Equation 2 in the reference frame comoving with the PSM [20]. We assume that the intrinsic frequency at a distance x to the arrest front is $\omega(x) = \omega_A(1 - e^{-x/\sigma})/(1 - e^{-L/\sigma})$, where x is a continuous variable and $\omega_A = 2\pi/T_A$ is the frequency of the individual oscillators in the posterior PSM. σ is the decay length of the frequency profile, measuring the characteristic distance over which the frequency decreases from high to low values, and L is the distance between the posterior end of the notochord and the arrest front of the oscillations. The continuum description relates the position x of the center of a wave of gene expression with its wavelength λ (Figure 4A) through the expression [20]

$$x = \sigma \ln\left[\frac{2\sigma \sinh(\lambda/2\sigma)}{S(1 - e^{-L/\sigma}) + \lambda e^{-L/\sigma}}\right], \quad (3)$$

where S is the arrested segment length. Note that the patterns of expression described by Equation 3 are not sensitive to spatial variation in coupling strength or delay. Fits of the theory to our *deltaC* stripe wavelength measurements were done by a total least square method, and error bars for S and σ were calculated by a bootstrap method. To allow an intuitive visualization of the results and comparison with potential results in different species, in Figures 4B and 4C we show the results normalized by the length L, for which we defined the normalized parameters $\rho = \sigma/L$ and $s = S/L$.

Fit of Somitogenesis Period versus DAPT Treatment Concentration

To relate the coupling strength ε in Equation 1 to the concentration n of the DAPT treatment, we first assume [13] that DAPT suppresses Notch signaling following Michaelis-Menten kinetics, [Notch] $\sim 1/(1 + n/n_0)$, where n_0 is the DAPT concentration that halves Notch signaling. The assumption of a linear relation of coupling strength to the level of Notch signaling, and that saturating DAPT completely blocks coupling [13], then yields $\varepsilon(n) = B/(1 + n/n_0)$, where B is a constant related to the wild-type level of Notch receptor expression. Following previous work, we assume that DAPT does not affect T_A over relevant time scales [13, 15]. Starting from Equation 1, a relation between period of oscillation and the level of DAPT treatment can be derived. Including a factor 100 to express the result as a percentage and assuming that the coupling delay lies on the second branch (Figure 5B), this relation is

$$\frac{T(n)}{T_u}\% = 100\frac{nT_A/T_u + Q}{n + Q}, \quad (4)$$

$$Q = n_0(1 + BT_A). \quad (5)$$

$T_u = T(0)$ is the period of untreated wild-type embryos. The parameters n_0 and B appear only through the combination Q defined in Equation 5. From the fit of Equation 4 to the data in Figure 5A we obtain $Q = 7.5 \pm 3.5$ μM. Using this value of Q we can estimate the coupling strength $\varepsilon = \varepsilon(0) = B = 0.07 \pm 0.04$ min^{-1} and the coupling delay $\tau = 21 \pm 2$ min.

Numerical Simulations of the Delayed Coupling Theory

For the simulations in this work we used a hexagonal two-dimensional lattice that has the same average shape and size as the experimental conditions. We solved the DCT equations by using parameters that we estimated in this work for the wild-type zebrafish. We measured a cell size of 7 pixels and used this as the size of single cells in the simulated patterns. Other parameters are the decay length of the frequency profile [20] $\sigma = 27$ cell diameters, the autonomous frequency of oscillators at the posterior boundary $\omega_A = 0.2205$ min^{-1}, the coupling strength $\varepsilon = 0.07$ min^{-1}, the coupling delay $\tau = 20.75$ min, and the arrest front velocity $v = 0.249$ cell diameters/min. Fluctuations were introduced with a noise term of strength $\eta = 0.02$ min^{-1}.

Autocorrelation Function

In this work we introduce a spatial autocorrelation function to measure disorder in gene expression patterns under different experimental conditions. We compute the autocorrelation function in a box from the anterior-most region of the PSM, where the most striking features of the expression patterns of wild-type, mutant, and also the Mib overexpression experiments are observed (Figure 6A). We define the autocorrelation function of the observed fluorescence intensity $I(x)$ as

$$C(\delta) = \langle I(x)I(x + \delta)\rangle \quad (6)$$

where the position x is measured from the anterior border of the box along the anteroposterior axial direction, and the brackets denote an average over space along the same axial direction followed by an average across the lateral direction. The autocorrelation is a function of the distance δ between two points in the pattern. Peaks of this function occur at distances where the intensity of the pattern is on average similar, as for example in consecutive stripes or interstripes of the cyclic gene expression patterns.

Supplemental Information

Supplemental Information includes seven figures, one table, Supplemental Experimental Procedures, and three movies and can be found with this article online at doi:10.1016/j.cub.2010.06.034.

Acknowledgments

The authors would like to thank the Max Planck Institute of Molecular Cell Biology and Genetics (MPI-CBG) fish, light microscopy, and sequencing facilities, the Dresden fish community, members of the Oates and Jülicher groups for discussion, and L. Rhode, I. Riedel-Kruse, J. Howard, C.-P. Heisenberg, and J. Pecreaux for critical comments on the manuscript. This work was funded by the Max Planck Society and by the European Research Council (ERC) under the European Communities Seventh Framework Programme (FP7/2007-2013) / ERC Grant no. 207634.

Received: March 5, 2010
Revised: May 12, 2010
Accepted: June 2, 2010
Published online: July 15, 2010

References

1. Winfree, A.T. (1967). Biological rhythms and the behavior of populations of coupled oscillators. J. Theor. Biol. *16*, 15–42.
2. Kuramoto, Y. (1984). Chemical Oscillations, Waves and Turbulence (Berlin: Springer Verlag).
3. Taylor, A.F., Tinsley, M.R., Wang, F., Huang, Z., and Showalter, K. (2009). Dynamical quorum sensing and synchronization in large populations of chemical oscillators. Science *323*, 614–617.
4. Walker, T.J. (1969). Acoustic synchrony: Two mechanisms in the snowy tree cricket. Science *166*, 891–894.

5. Buck, J. (1988). Synchronous rhythmic flashing of fireflies. II. Q. Rev. Biol. *63*, 265–289.
6. Schuster, H.P., and Wagner, G. (1989). Mutual entrainment of two limit cycle oscillators with time delayed coupling. Progress of Theoretical Physics *81*, 939–945.
7. Yeung, S., and Strogatz, S. (1999). Time delay in the Kuramoto model of coupled oscillators. Phys. Rev. Lett. *82*, 648–651.
8. Wünsche, H.J., Bauer, S., Kreissl, J., Ushakov, O., Korneyev, N., Henneberger, F., Wille, E., Erzgräber, H., Peil, M., Elsässer, W., and Fischer, I. (2005). Synchronization of delay-coupled oscillators: A study of semiconductor lasers. Phys. Rev. Lett. *94*, 163901.
9. Lewis, J. (2003). Autoinhibition with transcriptional delay: A simple mechanism for the zebrafish somitogenesis oscillator. Curr. Biol. *13*, 1398–1408.
10. Horikawa, K., Ishimatsu, K., Yoshimoto, E., Kondo, S., and Takeda, H. (2006). Noise-resistant and synchronized oscillation of the segmentation clock. Nature *441*, 719–723.
11. Masamizu, Y., Ohtsuka, T., Takashima, Y., Nagahara, H., Takenaka, Y., Yoshikawa, K., Okamura, H., and Kageyama, R. (2006). Real-time imaging of the somite segmentation clock: Revelation of unstable oscillators in the individual presomitic mesoderm cells. Proc. Natl. Acad. Sci. USA *103*, 1313–1318.
12. Palmeirim, I., Henrique, D., Ish-Horowicz, D., and Pourquié, O. (1997). Avian hairy gene expression identifies a molecular clock linked to vertebrate segmentation and somitogenesis. Cell *91*, 639–648.
13. Riedel-Kruse, I.H., Müller, C., and Oates, A.C. (2007). Synchrony dynamics during initiation, failure, and rescue of the segmentation clock. Science *317*, 1911–1915.
14. Schröter, C., Herrgen, L., Cardona, A., Brouhard, G.J., Feldman, B., and Oates, A.C. (2008). Dynamics of zebrafish somitogenesis. Dev. Dyn. *237*, 545–553.
15. Jiang, Y.J., Aerne, B.L., Smithers, L., Haddon, C., Ish-Horowicz, D., and Lewis, J. (2000). Notch signalling and the synchronization of the somite segmentation clock. Nature *408*, 475–479.
16. Ozbudak, E.M., and Lewis, J. (2008). Notch signalling synchronizes the zebrafish segmentation clock but is not needed to create somite boundaries. PLoS Genet. *4*, e15.
17. Giudicelli, F., Ozbudak, E.M., Wright, G.J., and Lewis, J. (2007). Setting the tempo in development: An investigation of the zebrafish somite clock mechanism. PLoS Biol. *5*, e150.
18. Heuss, S.F., Ndiaye-Lobry, D., Six, E.M., Israël, A., and Logeat, F. (2008). The intracellular region of Notch ligands Dll1 and Dll3 regulates their trafficking and signaling activity. Proc. Natl. Acad. Sci. USA *105*, 11212–11217.
19. Leier, A., Marquez-Lago, T.T., and Burrage, K. (2008). Generalized binomial tau-leap method for biochemical kinetics incorporating both delay and intrinsic noise. J. Chem. Phys. *128*, 205107.
20. Morelli, L.G., Ares, S., Herrgen, L., Schröter, C., Jülicher, F., and Oates, A.C. (2009). Delayed coupling theory of vertebrate segmentation. HFSP J. *3*, 55–66.
21. Kaern, M., Menzinger, M., and Hunding, A. (2000). Segmentation and somitogenesis derived from phase dynamics in growing oscillatory media. J. Theor. Biol. *207*, 473–493.
22. Jaeger, J., and Goodwin, B.C. (2001). A cellular oscillator model for periodic pattern formation. J. Theor. Biol. *213*, 171–181.
23. Uriu, K., Morishita, Y., and Iwasa, Y. (2009). Traveling wave formation in vertebrate segmentation. J. Theor. Biol. *257*, 385–396.
24. Cinquin, O. (2007). Repressor dimerization in the zebrafish somitogenesis clock. PLoS Comput. Biol. *3*, e32.
25. Tiedemann, H.B., Schneltzer, E., Zeiser, S., Rubio-Aliaga, I., Wurst, W., Beckers, J., Przemeck, G.K., and Hrabé de Angelis, M. (2007). Cell-based simulation of dynamic expression patterns in the presomitic mesoderm. J. Theor. Biol. *248*, 120–129.
26. Cooke, J., and Zeeman, E.C. (1976). A clock and wavefront model for control of the number of repeated structures during animal morphogenesis. J. Theor. Biol. *58*, 455–476.
27. Cooke, J. (1981). The problem of periodic patterns in embryos. Philos. Trans. R. Soc. Lond. B Biol. Sci. *295*, 509–524.
28. Gomez, C., Ozbudak, E.M., Wunderlich, J., Baumann, D., Lewis, J., and Pourquié, O. (2008). Control of segment number in vertebrate embryos. Nature *454*, 335–339.
29. Herrgen, L., Schröter, C., Bajard, L., and Oates, A.C. (2009). Multiple embryo time-lapse imaging of zebrafish development. Methods Mol. Biol. *546*, 243–254.
30. Jülich, D., Hwee Lim, C., Round, J., Nicolaije, C., Schroeder, J., Davies, A., Geisler, R., Lewis, J., Jiang, Y.J., and Holley, S.A.; Tübingen 2000 Screen Consortium. (2005). beamter/deltaC and the role of Notch ligands in the zebrafish somite segmentation, hindbrain neurogenesis and hypochord differentiation. Dev. Biol. *286*, 391–404.
31. van Eeden, F.J., Granato, M., Schach, U., Brand, M., Furutani-Seiki, M., Haffter, P., Hammerschmidt, M., Heisenberg, C.P., Jiang, Y.J., Kane, D.A., et al. (1996). Mutations affecting somite formation and patterning in the zebrafish, Danio rerio. Development *123*, 153–164.
32. Oates, A.C., and Ho, R.K. (2002). Hairy/E(spl)-related (Her) genes are central components of the segmentation oscillator and display redundancy with the Delta/Notch signaling pathway in the formation of anterior segmental boundaries in the zebrafish. Development *129*, 2929–2946.
33. Oates, A.C., Mueller, C., and Ho, R.K. (2005). Cooperative function of deltaC and her7 in anterior segment formation. Dev. Biol. *280*, 133–149.
34. Jiang, Y.J., Brand, M., Heisenberg, C.P., Beuchle, D., Furutani-Seiki, M., Kelsh, R.N., Warga, R.M., Granato, M., Haffter, P., Hammerschmidt, M., et al. (1996). Mutations affecting neurogenesis and brain morphology in the zebrafish, Danio rerio. Development *123*, 205–216.
35. Dequéant, M.L., and Pourquié, O. (2008). Segmental patterning of the vertebrate embryonic axis. Nat. Rev. Genet. *9*, 370–382.
36. Sawada, A., Fritz, A., Jiang, Y.J., Yamamoto, A., Yamasu, K., Kuroiwa, A., Saga, Y., and Takeda, H. (2000). Zebrafish Mesp family genes, mesp-a and mesp-b are segmentally expressed in the presomitic mesoderm, and Mesp-b confers the anterior identity to the developing somites. Development *127*, 1691–1702.
37. Konopka, R.J., and Benzer, S. (1971). Clock mutants of Drosophila melanogaster. Proc. Natl. Acad. Sci. USA *68*, 2112–2116.
38. Bruce, V.G. (1972). Mutants of the biological clock in Chlamydomonas reinhardi. Genetics *70*, 537–548.
39. Feldman, J.F., and Hoyle, M.N. (1973). Isolation of circadian clock mutants of Neurospora crassa. Genetics *75*, 605–613.
40. Vitaterna, M.H., King, D.P., Chang, A.M., Kornhauser, J.M., Lowrey, P.L., McDonald, J.D., Dove, W.F., Pinto, L.H., Turek, F.W., and Takahashi, J.S. (1994). Mutagenesis and mapping of a mouse gene, Clock, essential for circadian behavior. Science *264*, 719–725.
41. Momiji, H., and Monk, N.A. (2009). Oscillatory Notch-pathway activity in a delay model of neuronal differentiation. Phys. Rev. E Stat. Nonlin. Soft Matter Phys. *80*, 021930.
42. Shimizu, K., Chiba, S., Hosoya, N., Kumano, K., Saito, T., Kurokawa, M., Kanda, Y., Hamada, Y., and Hirai, H. (2000). Binding of Delta1, Jagged1, and Jagged2 to Notch2 rapidly induces cleavage, nuclear translocation, and hyperphosphorylation of Notch2. Mol. Cell. Biol. *20*, 6913–6922.
43. Itoh, M., Kim, C.H., Palardy, G., Oda, T., Jiang, Y.J., Maust, D., Yeo, S.Y., Lorick, K., Wright, G.J., Ariza-McNaughton, L., et al. (2003). Mind bomb is a ubiquitin ligase that is essential for efficient activation of Notch signaling by Delta. Dev. Cell *4*, 67–82.
44. Goldbeter, A., and Pourquié, O. (2008). Modeling the segmentation clock as a network of coupled oscillations in the Notch, Wnt and FGF signaling pathways. J. Theor. Biol. *252*, 574–585.
45. González, A., and Kageyama, R. (2009). Hopf bifurcation in the presomitic mesoderm during the mouse segmentation. J. Theor. Biol. *259*, 176–189.
46. Uriu, K., Morishita, Y., and Iwasa, Y. (2010). Synchronized oscillation of the segmentation clock gene in vertebrate development. J. Math. Biol. *61*, 207–229.
47. Aton, S.J., Colwell, C.S., Harmar, A.J., Waschek, J., and Herzog, E.D. (2005). Vasoactive intestinal polypeptide mediates circadian rhythmicity and synchrony in mammalian clock neurons. Nat. Neurosci. *8*, 476–483.
48. Renn, S.C., Park, J.H., Rosbash, M., Hall, J.C., and Taghert, P.H. (1999). A pdf neuropeptide gene mutation and ablation of PDF neurons each cause severe abnormalities of behavioral circadian rhythms in Drosophila. Cell *99*, 791–802.
49. Shimojo, H., Ohtsuka, T., and Kageyama, R. (2008). Oscillations in notch signaling regulate maintenance of neural progenitors. Neuron *58*, 52–64.
50. Plikus, M.V., and Chuong, C.M. (2008). Complex hair cycle domain patterns and regenerative hair waves in living rodents. J. Invest. Dermatol. *128*, 1071–1080.
51. Westerfield, M. (2000). The Zebrafish Book. A Guide for the Laboratory Use of Zebrafish (Danio rerio), 4th Edition (Eugene, OR: University of Oregon Press).
52. Holley, S.A., Geisler, R., and Nüsslein-Volhard, C. (2000). Control of her1 expression during zebrafish somitogenesis by a delta-dependent

oscillator and an independent wave-front activity. Genes Dev. *14*, 1678–1690.

53. Holley, S.A., Jülich, D., Rauch, G.J., Geisler, R., and Nüsslein-Volhard, C. (2002). her1 and the notch pathway function within the oscillator mechanism that regulates zebrafish somitogenesis. Development *129*, 1175–1183.
54. Brand, M., Heisenberg, C.P., Jiang, Y.J., Beuchle, D., Lun, K., Furutani-Seiki, M., Granato, M., Haffter, P., Hammerschmidt, M., Kane, D.A., et al. (1996). Mutations in zebrafish genes affecting the formation of the boundary between midbrain and hindbrain. Development *123*, 179–190.
55. Heisenberg, C.P., Brand, M., Jiang, Y.J., Warga, R.M., Beuchle, D., van Eeden, F.J., Furutani-Seiki, M., Granato, M., Haffter, P., Hammerschmidt, M., et al. (1996). Genes involved in forebrain development in the zebrafish, Danio rerio. Development *123*, 191–203.
56. Grandel, H., Lun, K., Rauch, G.J., Rhinn, M., Piotrowski, T., Houart, C., Sordino, P., Küchler, A.M., Schulte-Merker, S., Geisler, R., et al. (2002). Retinoic acid signalling in the zebrafish embryo is necessary during pre-segmentation stages to pattern the anterior-posterior axis of the CNS and to induce a pectoral fin bud. Development *129*, 2851–2865.
57. Zhang, C., Li, Q., Lim, C.H., Qiu, X., and Jiang, Y.J. (2007). The characterization of zebrafish antimorphic mib alleles reveals that Mib and Mind bomb-2 (Mib2) function redundantly. Dev. Biol. *305*, 14–27.